Dalton Transactions

ROYAL SOCIETY OF CHEMISTRY

PAPER

View Article Online
View Journal | View Issue

Cite this: *Dalton Trans.*, 2024, **53**, 12090

β-$CsHg_2I_5$, a compound with rare $[Hg_2I_5]$ dimers and large optical anisotropy†

Yingying Kong,‡[a,b] Hongshan Wang,‡[b] Wang Zhao,[b] Qi Sun,[b] Junjie Li *[b] and Shilie Pan *[a,b]

Hg-based compounds show abundant structural diversity and distinguished properties. Herein, a new phase transition compound $CsHg_2I_5$ was reported. The high-temperature phase β-$CsHg_2I_5$ with rare $[Hg_2I_5]$ dimers was synthesized by the flux method at 573 K, and it shows a reversible phase transition at a low temperature of ~100 K to form the low-temperature phase α-$CsHg_2I_5$. The two phases crystallize in the same $P2_1/c$ space group, with different crystal structures. β-$CsHg_2I_5$ is composed of rare $[Hg_2I_5]$ dimers and $[CsI_{11}]$ polyhedral units, while α-$CsHg_2I_5$ is composed of $[Hg_4I_{11}]$ and $[CsI_{10}]$ units. The experimental band gap of β-$CsHg_2I_5$ was found to be 2.58 eV. Owing to the presence of $[Hg_2I_5]_\infty$ pseudo-layers, β-$CsHg_2I_5$ exhibits large optical anisotropy with a calculated birefringence of 0.132@1064 nm. Meanwhile, β-$CsHg_2I_5$ is a congruent compound and the congruent point is ~481 K. Theoretical calculations indicate that the rare $[Hg_2I_5]$ dimer is a nonlinear active unit, which can be used as a new fundamental building block for the design of advanced nonlinear optical materials. Moreover, a CsI–HgI_2 pseudo-binary diagram was drawn. The results enrich the structural diversity of Hg-based halides and give some insights into the development of new functional materials based on rare $[Hg_2I_5]$ dimers.

Received 26th May 2024,
Accepted 25th June 2024

DOI: 10.1039/d4dt01536c

rsc.li/dalton

Introduction

The development of both new functional materials and structural chemistry is highly dependent on the discovery of new compounds with distinctive structures and physiochemical properties.[1–6] Metal halides, with abundant structural diversities and adjustable optical performances,[7,8] are an important class of photoelectronic functional materials that are applied in the fields of photoelectric detection,[9,10] nonlinear optics (NLO),[11–14] infrared window materials,[15–17] new energy materials[18] and so on. Over the past decades, many metal halides with multiple structures and distinguished properties like $CsGeQ_3$ (Q = Br and I),[19,20] $NaSb_3F_{10}$,[21] and $K_2SbF_2Cl_3$[22] were rationally designed and fabricated experimentally by the high-temperature solid state/solution method or wet chemistry routes.[20–24]

Recently, Hg-based halides have received considerable attention because of their potential applications in advanced optoelectronic fields, and several Hg-based halides have been developed.[25–29] For example, Wu and coworkers reported the syntheses of Ag_2HgI_4 and $NH_4HgBr_3{\cdot}H_2O$ by wet chemical routes in 2021.[25–27] Among them, $NH_4HgBr_3{\cdot}H_2O$ shows a quasi-one-dimensional (1D) crystal structure composed of $[HgBr_3]$ chains and aligned $[HgBr_4]$ tetrahedral units, resulting in excellent optical properties, including a strong SHG (28 × KDP), a large birefringence (0.183 at 1064 nm) and a high laser-induced damage threshold (52.7 × $AgGaS_2$).[25] Remarkably, the 6s and 6p orbital energies of Hg with a unique d^{10} electronic configuration are close to each other,[30,31] giving rise to various coordination modes between Hg and halides, such as linear $[HgQ_2]$ (Q = halide elements), planar $[HgQ_3]$ and tetrahedral $[HgQ_4]$ units.[32,33] Similar to borates, the basic structural units can be further linked with each other to build new fundamental building block (FBB) groups theoretically.[34–37] Nevertheless, the $[Hg_xQ_y]$ units (Q = halide elements; x and y = integers and ≥2) are quite rare in the known Hg-based compounds, far less than the number of $[B_xO_y]$ units (x and y = integers and ≥2) in the borates.[38–40]

In this work, an experimental investigation was carried out in the Cs–Hg–I system, and a high-temperature phase ternary Hg-based halide β-$CsHg_2I_5$ was successfully synthesized by a high-temperature solution reaction. Interestingly, the

[a]*College of Chemistry, Zhengzhou University, Zhengzhou 450001, China*
[b]*Research Center for Crystal Materials; State Key Laboratory of Functional Materials and Devices for Special Environmental Conditions; Xinjiang Key Laboratory of Functional Crystal Materials; Xinjiang Technical Institute of Physics and Chemistry, Chinese Academy of Sciences, 40-1 South Beijing Road, Urumqi 830011, China. E-mail: lijunjie@ms.xjb.ac.cn, slpan@ms.xjb.ac.cn*

†Electronic supplementary information (ESI) available. CCDC 2358225 and 2358226. For ESI and crystallographic data in CIF or other electronic format see DOI: https://doi.org/10.1039/d4dt01536c

‡These authors contributed equally to this work.

compound exhibits a reversible phase transition at a low temperature of ~100 K during single crystal X-ray diffraction measurements, resulting in a low-temperature phase structure (α-$CsHg_2I_5$). Based on the structural investigations in the Inorganic Crystal Structure Database (ICSD version 5.0.0 (build 20230418–1517)), β-$CsHg_2I_5$ contains an unprecedented [Hg_2I_5] dimer and is composed of [Hg_2I_5] pseudo-layers and a Cs–I framework built by [CsI_{11}] polyhedral units, different from the [CsI_{10}] and [Hg_4I_{11}] containing three-dimensional (3D) crystal structure in α-$CsHg_2I_5$. Notably, β-$CsHg_2I_5$ is a congruent compound with a melting point of ~481 K. The experimental and calculated results show that β-$CsHg_2I_5$ is a direct band gap compound with an experimental optical band gap of 2.58 eV, and it has a large birefringence of 0.132@1064 nm. Theoretical calculations unveil that the band gap and birefringence in the compound mainly originate from the [Hg_2I_5] dimers.

Experimental section

Reagents

The raw materials CsI and HgI_2 with a purity of 99.9% were purchased from Aladdin Industrial Corporation. All the raw reagents were stored in a dry Ar-filled glove box with controlled oxygen and moisture levels below 0.1 ppm and used without further purification.

Syntheses

The single crystal of high temperature phase β-$CsHg_2I_5$ for single-crystal X-ray diffraction (XRD) measurement was synthesized by the flux method.[41–43] First, 0.5 g of starting materials CsI and HgI_2 with a molar ratio of 1 : 1 were weighed and filled in a quartz tube with an inner diameter of 10 mm, and the quartz tube was further sealed by a hydroxide flame under a pressure of 10^{-3} Pa. Afterwards, the quartz tube was placed in a programmable muffle furnace, heated to 573 K over 10 h, held at this temperature for 36 h, and then cooled to room temperature at a rate of 10 K h^{-1}. Finally, yellowish transparent β-$CsHg_2I_5$ single crystals were harvested.

The pure phase polycrystalline powder samples of β-$CsHg_2I_5$ were synthesized by the high-temperature solution method. The stoichiometric ratio raw materials CsI and HgI_2 were weighed and sealed in quartz tubes. The samples were rapidly heated to 573 K from room temperature and maintained at this temperature for 10 h, cooled to 373 K at a rate of 20 K h^{-1}, and then naturally cooled down to room temperature. Finally, yellow $CsHg_2I_5$ pure phase samples were achieved.

Single crystal structure determination

The yellowish transparent single crystals were observed under an optical microscope for structural determination with a Bruker D8 Venture diffractometer using monochromatic Mo Kα radiation (λ = 0.71073 Å). The diffraction data collection was carried out at room temperature (~300 K) for β-$CsHg_2I_5$ and 100 K for low-temperature phase α-$CsHg_2I_5$. The single crystal structures were solved by direct methods and optimized using the SHELXTL crystallographic software package.[44,45] PLATON software was utilized to confirm the lack of higher symmetry in the crystal structures.[46]

Powder X-ray diffraction

Powder XRD measurements of β-$CsHg_2I_5$ were carried out on a Bruker D2 Phaser diffractometer equipped with a diffracted beam monochromator set for Cu Kα radiation (λ = 1.5418 Å), and the diffraction patterns were recorded from 10 to 70° (2θ).

Energy dispersive X-ray spectroscopy (EDS)

Elemental analysis of β-$CsHg_2I_5$ was performed using a field emission scanning electron microscope (FE-SEM, JEOL JSM-7610F Plus, Japan) at 298 K with an energy dispersive X-ray spectrometer (Oxford, X-Max 50) operated at 5 kV.

Raman spectrum

The Raman spectrum of β-$CsHg_2I_5$ single crystals was recorded using a LABRAM HR Evolution spectrometer equipped with a CCD detector (cooling temperature: 218 K) under 532 nm radiation (beam diameter: 35 μm; power: 60 mW) from a diode laser and acquired from 500 to 50 cm^{-1} (20–200 μm). The integration time was set to 5 s.

UV-vis-NIR diffuse reflectance spectrum

The diffuse reflectance spectrum of pure phase β-$CsHg_2I_5$ was recorded using a Shimadzu SolidSpec-3700DUV spectrophotometer at room temperature, and the reflectance spectral data were converted to absorption spectral data using the Kubelka–Munk formula: $\alpha/S = (1 - R)2/(2R)$, (R = reflectance; α = absorption; and S = scattering).[47–50]

Thermal analysis

Differential scanning calorimetry (DSC) analysis of β-$CsHg_2I_5$ was performed using a NETZSCH STA 449F3 simultaneous thermal analyzer. Before the measurement, 15 mg of powder samples were sealed in a quartz tube. The samples were heated to 573 K from room temperature and then cooled down to room temperature with a heating/cooling rate of 5 K min^{-1}.

Theoretical calculations

First-principles calculations based on density functional theory (DFT) for β-$CsHg_2I_5$ were carried out using the CASTEP software package.[51–54] The exchange–correlation functional used was the Perdew–Burke–Ernzerhof (PBE) functional within the generalized gradient approximation (GGA).[55] The kinetic energy cutoff was set to 500 eV. The k-points of the Monkhorst–Pack grids in the Brillouin zone were set to 5 × 3 × 3. The refractive index was investigated using the Kramers–Kronig relation. In addition, the response electron distribution anisotropy (REDA, ζ) index was utilized to reflect the birefringence contribution of each unit, and

the response charge density can be derived from the following equation:[56]

$$\zeta = \sum_{g} \left[\frac{N_c Z_a \Delta\rho^b}{n_1 E_o} \right]_g$$

where N_c is the number of nearest-neighbor coordination sites, Z_a represents the formal charge of the anion, $\Delta\rho^b = \rho^b_{max} - \rho^b_{min}$, where ρ^b_{max} and ρ^b_{min} are the maximum and minimum values of the covalent electron density for covalent bonding in the optical principal axis of the crystal, respectively, n_1 is the minimum refractive index, and E_o represents the optical band gap. Moreover, based on the Voigt–Reuss–Hill method, the bulk modulus of β-$CsHg_2I_5$ was calculated using CASTEP.

Results and discussion

β-$CsHg_2I_5$ crystallizes in the monoclinic space group $P2_1/c$ (no. 14) with cell parameters a = 8.8094(14) Å, b = 11.4931(17) Å, c = 14.075(2) Å, β = 107.073(6) °, and Z = 4. In the asymmetric unit of β-$CsHg_2I_5$, there is one crystallographically independent Cs atom, two Hg atoms, and five I atoms. Each Cs atom is linked to eleven I atoms to form a $[CsI_{11}]$ polyhedron with bond lengths of $d_{Cs\text{-}I}$ = 3.915(2)–4.481(33) Å (Fig. 1a), and the Hg atoms are three-coordinated with I to build planar $[HgI_3]$ units with $d_{Hg\text{-}I}$ = 2.465(2) to 3.122(3) Å (Fig. 1b and c). The Raman spectrum confirms the Cs–I (114 cm^{-1}) and Hg–I (138 cm^{-1}) chemical bonding in the compound (Fig. S1†). The $[CsI_{11}]$ polyhedral units are interconnected by sharing I atoms to build a tunnel-like 3D Cs–I structure framework (Fig. 1e). Each of the two $[HgI_3]$ units are further connected with each other by corner-sharing to construct a rare $[Hg_2I_5]$ dimer (Fig. 1d). The formed $[Hg_2I_5]$ dimers are isolated from each other (Fig. 1f), which are in the channels of the 3D Cs–I framework, resulting in the final 3D crystal structure (Fig. 1g). The calculated bond valence sums (BVSs) (Cs: 0.84, Hg: 2.28–2.38, I: 0.85–1.19) verify the rationality of the crystal structure.

It is worth noting that when the measured temperature is reduced to about 100 K, the β phase $CsHg_2I_5$ shows a reversible phase transition to α phase $CsHg_2I_5$ (Fig. S2†). The two phases crystallize in the same monoclinic space group $P2_1/c$ (no. 14), but with different cell parameters and structures. The cell parameters of α-$CsHg_2I_5$ are a = 14.0019(16) Å, b = 11.4545(14) Å, c = 19.067(3) Å, β = 117.911(4)°, and Z = 8. In the asymmetric unit of α-$CsHg_2I_5$, there are two crystallographically independent Cs atoms, four Hg atoms, and ten I atoms. Each Cs atom is linked to ten I atoms to form a $[CsI_{10}]$ polyhedron with bond lengths of $d_{Cs\text{-}I}$ = 3.880(8)–4.509(9) Å (Fig. S3a†), while Hg atoms form planar $[HgI_3]$ and tetrahedral $[HgI_4]$ units that are different from the formed $[Hg_2I_5]$ dimers in β-$CsHg_2I_5$.[57] The $[CsI_{10}]$ polyhedral units are interconnected by sharing I atoms to build a tunnel-like 3D Cs–I structure framework (Fig. S3e†). Each of the two $[HgI_3]$ and two $[HgI_4]$ units is further connected with each other by corner-sharing to construct a rare $[Hg_4I_{11}]$ group (Fig. S3d†). The formed $[Hg_4I_{11}]$ groups are interconnected, extended along the b direction (Fig. S3f†), and located in the channels of the 3D Cs–I framework, resulting in the final 3D crystal structure of α-$CsHg_2I_5$ (Fig. S3g†).

The detailed crystallographic data of α-$CsHg_2I_5$ and β-$CsHg_2I_5$, including structure and refinement parameters, atomic coordinates, equivalent isotropic displacement parameters, atomic bond valences, bond lengths, and bond angles are listed in Tables S1–S11.†

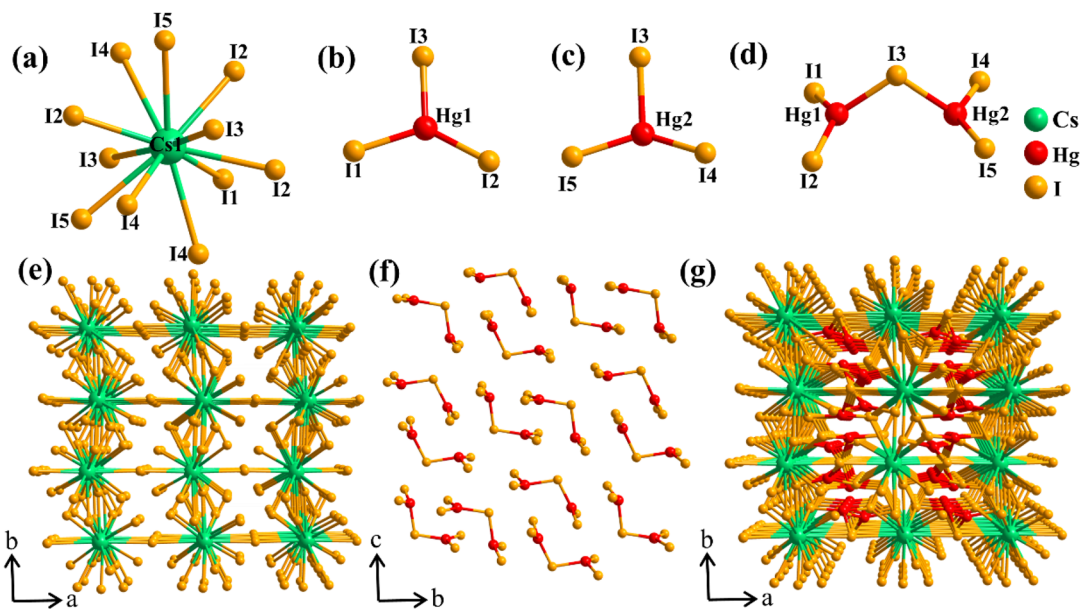

Fig. 1 (a–c) Coordination modes of Cs, Hg(1) and Hg(2); (d) the formed $[Hg_2I_5]$ dimer; (e) the formed Cs-I framework; (f) the resulting $[Hg_2I_5]$ pseudo-layer; and (g) the 3D crystal structure of β-$CsHg_2I_5$.

It is worth noting that Wells *et al.* investigated the CsI–HgI_2–H_2O system by a wet chemical route in 1892,[58] and described five Hg-based iodides, $CsHg_2I_5$, $Cs_2Hg_3I_8$, $CsHgI_3$ (possibly a hydrate), Cs_2HgI_4 and Cs_3HgI_5 in this system, but the crystallographic data were lacking. After that, Kirilenko *et al.* confirmed the existence of Cs_2HgI_4, $CsHgI_3$ and $CsHg_2I_5$ based on the differential-thermal and X-ray phase analysis.[59] In 1988, Christer and coworkers reinvestigated the system and the crystal structures of $Cs_2Hg_3I_8{\cdot}H_2O$ (*Cm*), Cs_2HgI_4 ($P2_1/m$) and Cs_3HgI_5 (*Pbca*) were first determined by diffractometer data.[60] Nevertheless, the crystal structures of $CsHgI_3$ and $CsHg_2I_5$ are still under investigation. In this work, the crystallographic information of α/β-$CsHg_2I_5$ was obtained by single crystal XRD. To clearly show the existent structures in the CsI–HgI_2 system, a CsI–HgI_2 pseudo-binary diagram containing seven cesium Hg iodides was drawn, as shown in Fig. 2a. Based on the structural investigations in ICSD, it can be seen that there are four types of coordination modes in the Hg-contained iodides, corresponding to four FBBs, $[Hg_2I_2]$,[61] $[HgI_2]$,[62] $[HgI_3]$, and $[HgI_4]$,[63] while the formed $[Hg_2I_5]$ dimer composed of two $[HgI_3]$ units in β-$CsHg_2I_5$ is first observed in the Hg-based system. In addition, statistical analyses indicate that most of the formed $[Hg_xI_y]$ units are isolated from each other (named 0D in Fig. 2b) in the compounds.

The EDS spectrum (Fig. 3a) shows the presence of Cs, Hg and I elements in the crystal with an atomic ratio of Cs : Hg : I = 1 : 1.63 : 4.53 (Table S12†), close to the results in the chemical formula of β-$CsHg_2I_5$, confirming the results of single crystal XRD. Meanwhile, the polycrystalline pure phase powder samples of β-$CsHg_2I_5$ were synthesized by the high-temperature solution method (see the details in the Experimental section). To check the structure and purity of the synthesized samples, the powder XRD pattern was characterized, and it is matched with the theoretical results that are derived from the β-$CsHg_2I_5$ CIF file using Mercury software. Moreover, the Rietveld refinement based on the powder XRD pattern was carried out using GSAS software, and the refined R_p and R_{wp} values were 5.33% and 6.99%, respectively, further confirming the crystal structure and the purity of the obtained polycrystalline samples. The results indicate the high purity of the obtained polycrystalline samples (Fig. 3b).

To detect the optical band gap, the UV-vis-NIR diffuse reflectance spectrum of β-$CsHg_2I_5$ was recorded and the absorption data were obtained using the Kubelka–Munk function.[64] The experimental band gap was determined to be 2.58 eV (Fig. 3c), comparable to the ones in Cs_2HgI_4 (2.34 eV),[63] $Cs_2Hg_3I_8{\cdot}H_2O$ (2.56 eV),[24] and Hg_2BrI_3 (2.60 eV).[65] To unveil the thermal behavior of β-$CsHg_2I_5$, a differential scanning calorimetry (DSC) test was conducted in a sealed system. As shown in Fig. S4,† there is an evident endothermic peak at 481 K during the heating process. To investigate the origin of the peak, the polycrystalline β-$CsHg_2I_5$ powder sample was heated to 523 K, maintained at this temperature for 30 h, and then cooled to room temperature in a muffle furnace. The XRD pattern of β-$CsHg_2I_5$ after melting agrees with the one before melting. To further confirm it, the powder XRD Rietveld refinement based on polycrystalline samples after melting was conducted. The refined R_p and R_{wp} values were 5.63% and 7.23%, respectively, demonstrating the crystal structure of β-$CsHg_2I_5$ after melting. The results demonstrate that β-$CsHg_2I_5$ is a congruent-melting compound (Fig. 3d), which is beneficial for crystal growth by the melting method.[66,67]

To understand the origin of optical properties, the band structure of β-$CsHg_2I_5$ was first computed using DFT calculations.[68–70] The optimized structure model and unit-cell parameters of β-$CsHg_2I_5$ are shown in Fig. S6,† and the bulk moduli (Table S13†) from the atomic model were calculated to be 9.89422 (Voigt), 7.99758 (Reuss), and 8.94950 (Hill). The band structure implies that β-$CsHg_2I_5$ is a direct band gap compound. The calculated GGA band gap is 2.14 eV (Fig. 4a), which is smaller than the experimental value (2.58 eV), due to the discontinuity in the underestimation of the GGA band gap caused by the exchange–correlation energy functional during DFT calculations.[71,72] The total and partial density of states (DOS) show that the top of the valence band (VB) is mainly dominated by the I-5p orbitals, and the bottom of the conduction band (CB) is occupied by the I-5s, I-5p and Hg-5s orbitals (Fig. 4b), implying that the optical band gap of β-$CsHg_2I_5$ is

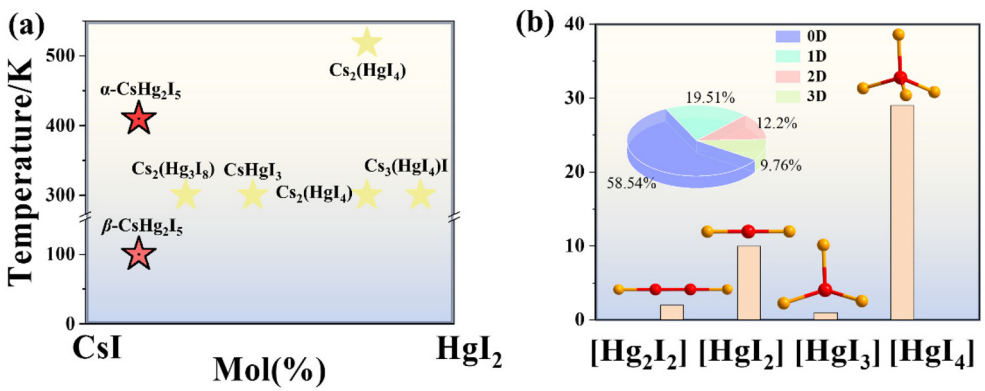

Fig. 2 (a) CsI–HgI_2 pseudo-binary diagram; (b) statistical analyses showing the formed $[Hg_xI_y]$ units and the dimensional distribution (inset) of the Hg-contained iodides in ICSD (ICSD version 5.0.0 (build 20230418–1517)).

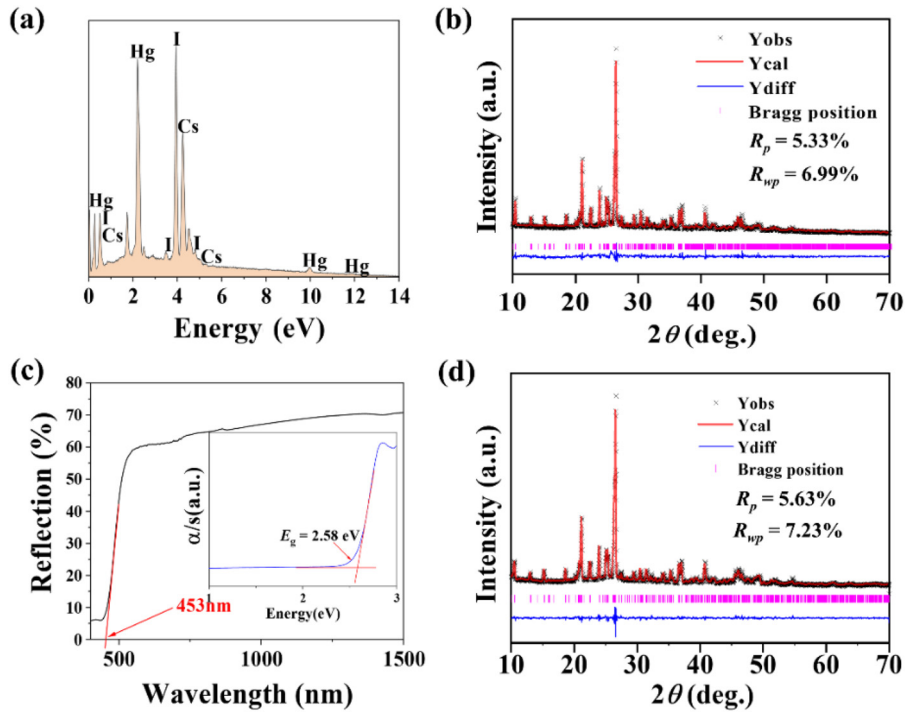

Fig. 3 (a) EDS spectrum; (b) the Rietveld refinement PXRD pattern before melting; (c) experimental band gap; (d) the Rietveld refinement PXRD pattern after melting of β-$CsHg_2I_5$.

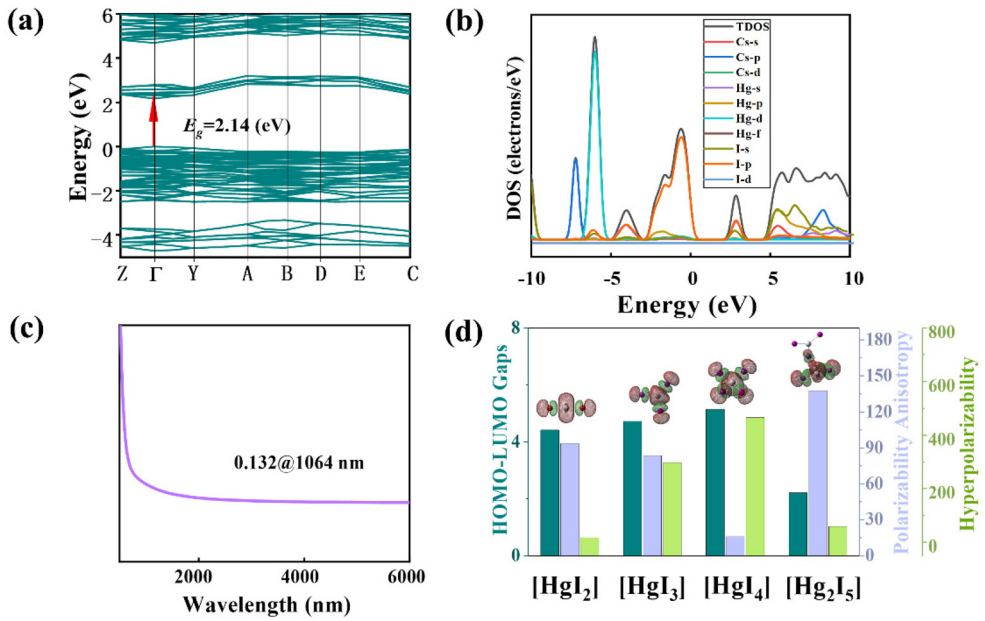

Fig. 4 (a) Calculated band structure; (b) total and partial density of states; (c) calculated birefringence of β-$CsHg_2I_5$; (d) the HOMO–LUMO energy gap, polarizability anisotropy and hyperpolarizability of $[HgI_2]$, $[HgI_3]$, $[HgI_4]$ and $[Hg_2I_5]$ units.

determined by the Hg–I bonding in the $[Hg_2I_5]$ dimers. Moreover, the planar unit usually exhibits large polarizability anisotropy. In β-$CsHg_2I_5$, the isolated $[Hg_2I_5]$ dimers are arranged in the *bc*-plane to form a $[Hg_2I_5]$ pseudo-layer (Fig. 1f) in the structure, which is conducive to inducing strong optical anisotropy. To check the optical anisotropy, the refractive indices of β-$CsHg_2I_5$ were investigated, and the birefringence Δn was calculated to be 0.132@1064 nm (Fig. 4c), far larger than the ones in Cu_2HgI_4 with $[HgI_4]$ (0.032@1064 nm),[29] Ag_2HgI_4 with $[HgI_4]$ (0.031@1064 nm) and

$RbHgI_3$ with $[HgI_4]$ (0.08@1064 nm).[28,29] To uncover the origin of birefringence in β-$CsHg_2I_5$, the bonding electron density difference ($\Delta\rho$) values of $[CsI_{11}]$ polyhedral and $[Hg_2I_5]$ units were calculated by the REDA method.[73] The results in Fig. S5† imply that the large birefringence in the compound mainly originates from the $[Hg_2I_5]$ dimers in the pseudo-layers.

To illustrate the fluctuations in the optical properties between the Hg–I units, the hyperpolarizability, HOMO–LUMO energy gap and polarizability anisotropy of $[HgI_2]$, $[HgI_3]$, $[HgI_4]$ and the $[Hg_2I_5]$ dimer were investigated using the Gaussian 09 software package.[74] As shown in Fig. 4d, the $[Hg_2I_5]$ dimer exhibits strong polarizability anisotropy and moderate hyperpolarizability. The results confirm that the $[Hg_2I_5]$ dimer can be used as a promising NLO-active unit for the design of new NLO materials. Meanwhile, it implies that the dimers or trimers of planar units can effectively enhance the optical anisotropy of Hg-based compounds.

Conclusions

In summary, a new phase transition compound $CsHg_2I_5$ was synthesized by the flux method. β-$CsHg_2I_5$ and α-$CsHg_2I_5$ phases crystallize in the same $P2_1/c$ space group, but show different structures. Owing to the presence of $[Hg_2I_5]$ pseudo-layers in β-$CsHg_2I_5$, a large birefringence ($\Delta n_{(cal.)}$ = 0.132@1064 nm) is achieved in the compound, indicating that constructing a dimer or trimer of planar units is a feasible strategy to enhance the optical anisotropy of Hg-based compounds. Meanwhile, the study of thermal behavior indicates that β-$CsHg_2I_5$ is a congruent compound with a relatively low melting point of ~481 K. Theoretical calculations show that β-$CsHg_2I_5$ is a direct band gap compound with a GGA band gap of 2.14 eV, close to the experimental value of 2.58 eV. In addition, theoretical calculation indicates that the $[Hg_2I_5]$ dimer could be a promising NLO-active unit for the design of new functional materials.

Data availability

Data will be made available upon request.

Conflicts of interest

There are no conflicts to declare.

Acknowledgements

This work was supported by the National Natural Science Foundation of China (22335007, 52002398, 61835014, 51972336) and Xinjiang Key Laboratory of Electronic Information Materials and Devices (2017D04029).

References

1 M. Mutailipu, M. Zhang, H. Wu, Z. Yang, Y. Shen, J. Sun and S. Pan, *Nat. Commun.*, 2018, **9**, 3089.
2 J. Chen, P. Yang, H. Yu, Z. Hu, J. Wang, Y. Wu and H. Wu, *ACS Mater. Lett.*, 2023, **5**, 1665–1671.
3 H. Wang, Y. Chu, X. Pan, Z. Yang, S. Pan and J. Li, *Mater. Today Phys.*, 2023, **38**, 101243.
4 J. Zhou, L. Wang, Y. Chu, H. Wang, S. Pan and J. Li, *Adv. Opt. Mater.*, 2023, **11**, 2300736.
5 L. Wang, C. Tu, J. Zhou, Y. Chu, Z. Yang, S. Pan and J. Li, *Adv. Opt. Mater.*, 2023, **12**, 2301634.
6 G. Deokar, N. S. Rajput, J. Li, F. L. Deepak, W. Ou-Yang, N. Reckinger, C. Bittencourt, J. F. Colomer and M. Jouiad, *Beilstein J. Nanotechnol.*, 2018, **9**, 1686–1694.
7 W. Li, L. Geng, C. Meng, S. Ma, B. Zhu, Y. Lan and Q. Wu, *Adv. Opt. Mater.*, 2023, **12**, 2302560.
8 Y. Song, S. Cui, Z. Qian, H. Yu, Z. Hu, J. Wang, Y. Wu and H. Wu, *Inorg. Chem. Front.*, 2022, **9**, 5932–5940.
9 D. Wang and G. Li, *Photonics Rev.*, 2022, **16**, 2100713.
10 S. Cui, Y. Chen, S. Tao, J. Cui, C. Yuan, N. Yu, H. Zhou, J. Yin and X. Zhang, *Eur. J. Inorg. Chem.*, 2020, **2020**, 2165–2169.
11 C. Zhang, X. Niu, Y. Wei, S. Zhou, D. Yang, Y. Wang, J. Wang and B. Zhang, *Rare Met.*, 2023, **43**, 395–401.
12 B. Cai, C. Chen, Y. Bai, Q. Shi, B. Zhang and Y. Wang, *Inorg. Chem.*, 2024, **63**, 6122–6126.
13 L. Wang, Q. Sun and J. Li, *Chin. J. Struct.*, 2023, **42**, 100013.
14 L. Wang, D. Chu, D. Yin, C. Xie, Z. Yang, J. Li and S. Pan, *Mater. Today Phys.*, 2023, **38**, 101245.
15 X. Lou, X. Jiang, B. Liu and G. Guo, *Small*, 2023, **20**, 2305711.
16 H. Wang, X. Pan, W. Zhao, Y. Chu and J. Li, *Inorg. Chem. Front.*, 2023, **10**, 6253–6261.
17 J. R. Glenn, J. B. Cho, Y. Wang, A. J. Craig, J. Zhang, M. Cribbs, S. S. Stoyko, K. E. Rosello, C. Barton, A. Bonnoni, P. GrimaGallardo, J. H. MacNeil, J. M. Rondinelli, J. I. Jang and J. A. Aitken, *Dalton Trans.*, 2021, **50**, 17524–17537.
18 G. Li, S. Guo, B. Xiang, S. Mei, Y. Zheng, X. Zhang, B. Gao, P. K. Chu and K. Huo, *Energy Mater.*, 2022, **2**, 200020.
19 T. Luo, Y. Xia, J. Huang, X. Huang, Z. Wu, Y. Chen, X. Xu, W. Xie, P. Liu and C. Hu, *CrystEngComm*, 2021, **23**, 4917–4922.
20 U. Jong, C. Yu, Y. Kye, Y. Choe, W. Hao and S. Li, *Inorg. Chem.*, 2019, **58**, 4134–4140.
21 G. Zhang, J. Qin, T. Liu, Y. Li, Y. Wu and C. Chen, *Appl. Phys. Lett.*, 2009, **95**, 261104.
22 Y. Huang, X. Meng, P. Gong, Z. Lin, X. Chen and J. Qin, *J. Mater. Chem. C*, 2015, **3**, 9588–9593.
23 G. Han, Y. Wang, B. Zhang and S. Pan, *Chem. – Eur. J.*, 2018, **24**, 17638–17650.
24 Q. Wu, Y. Huang, X. Meng, C. Zhong, X. Chen and J. Qin, *Dalton Trans.*, 2014, **43**, 8899–8904.
25 Q. Wu, C. Yang, X. Liu, J. Ma, F. Liang and Y. Du, *Mater. Today Phys.*, 2021, **21**, 100569.

26 Q. Wu, X. Meng, C. Zhong, X. Chen and J. Qin, *J. Am. Chem. Soc.*, 2014, **136**, 5683–5686.
27 C. Yang, X. Liu, C. Teng, X. Cheng, F. Liang and Q. Wu, *Mater. Today Phys.*, 2021, **19**, 100432.
28 Y. Li, Y. Ding, Y. Li, H. Liu, X. Meng, Y. Cong, J. Zhang, X. Li, X. Chen and J. Qin, *Crystals*, 2017, **7**, 148.
29 P. Gong, F. Liang, L. Kang and Z. Lin, *Chem. Mater.*, 2022, **34**, 5301–5310.
30 Y. Zhang, H. Wu, Z. Hu, J. Wang, Y. Wu and H. Yu, *Inorg. Chem. Front.*, 2022, **9**, 4075–4080.
31 X. Zhang, H. Wu, Z. Hu, J. Wang, Y. Wu and H. Yu, *Adv. Opt. Mater.*, 2023, **12**, 2301735.
32 Y. Chu, H. Wang, Q. Chen, X. Su, Z. Chen, Z. Yang, J. Li and S. Pan, *Adv. Funct. Mater.*, 2023, **34**, 2314933.
33 P. Gong, F. Liang, L. Kang, X. Chen, J. Qin, Y. Wu and Z. Lin, *Coord. Chem. Rev.*, 2019, **380**, 83–102.
34 M. Mutailipu, M. Zhang, B. Zhang, L. Wang, Z. Yang, X. Zhou and S. Pan, *Angew. Chem., Int. Ed.*, 2018, **57**, 6095–6099.
35 X. Wang, Y. Wang, B. Zhang, F. Zhang, Z. Yang and S. Pan, *Angew. Chem., Int. Ed.*, 2017, **56**, 14119–14123.
36 Y. Wang, B. Zhang, Z. Yang and S. Pan, *Angew. Chem., Int. Ed.*, 2018, **57**, 2150–2154.
37 G. Shi, Y. Wang, F. Zhang, B. Zhang, Z. Yang, X. Hou, S. Pan and K. R. Poeppelmeier, *J. Am. Chem. Soc.*, 2017, **139**, 10645–10648.
38 C. Li, X. Meng, Z. Li and J. Yao, *Coord. Chem. Rev.*, 2022, **453**, 214328.
39 H. Qiu, F. Li, C. Jin, Z. Yang, J. Li, S. Pan and M. Mutailipu, *Angew. Chem., Int. Ed.*, 2023, **63**, e202316194.
40 M. Mutailipu, M. Zhang, Z. Yang and S. Pan, *Acc. Chem. Res.*, 2019, **52**, 791–801.
41 J. Zhang, D. J. Clark, J. A. Brant, K. A. Rosmus, P. Grima, J. W. Lekse, J. I. Jang and J. A. Aitken, *Chem. Mater.*, 2020, **32**, 8947–8955.
42 J. Zhang, S. S. Stoyko, A. J. Craig, P. Grima, J. W. Kotchey, J. I. Jang and J. A. Aitken, *Chem. Mater.*, 2020, **32**, 10045–10054.
43 J. Zhou, Z. Fan, K. Zhang, Z. Yang, S. Pan and J. Li, *Mater. Horiz.*, 2023, **10**, 619–624.
44 G. M. Sheldrick, *Acta Crystallogr., Sect. A: Found. Crystallogr.*, 2007, **64**, 112–122.
45 Y. Chu, H. Wang, T. Abutukadi, Z. Li, M. Mutailipu, X. Su, Z. Yang, J. Li and S. Pan, *Small*, 2023, **19**, 2305074.
46 X. Dong, H. Huang, L. Huang, Y. Zhou, B. Zhang, H. Zeng, Z. Lin and G. Zou, *Angew. Chem., Int. Ed.*, 2024, **63**, e202318976.
47 L. Lin, X. Jiang, C. Wu, Z. Lin, Z. Huang, M. G. Humphrey and C. Zhang, *Dalton Trans.*, 2021, **50**, 7238–7245.
48 A. Abudurusuli, J. Huang, P. Wang, Z. Yang, S. Pan and J. Li, *Angew. Chem., Int. Ed.*, 2021, **60**, 24131–24136.
49 P. Wang, Y. Chu, A. Tudi, C. Xie, Z. Yang, S. Pan and J. Li, *Adv. Sci.*, 2022, **9**, 2106120.
50 X. Chai, M. Li, S. Lin, W. Chen, X. Jiang, B. Liu and G. Guo, *Small*, 2023, **19**, 2303847.
51 L. Wu, R. Zhang, Q. Jing, H. Huang, X. He, Z. Wang and Z. Chen, *Inorg. Chem. Front.*, 2023, **10**, 4496–4502.
52 Y. Han, C. Hu and J. Mao, *Small*, 2023, **20**, 2305828.
53 D. Chu, Y. Huang, C. Xie, E. Tikhonov, I. Kruglov, G. Li, S. Pan and Z. Yang, *Angew. Chem., Int. Ed.*, 2023, **62**, e202300581.
54 K. Chen, C. Lin, J. Chen, G. Yang, H. Tian, M. Luo, T. Yan, Z. Hu, J. Wang, Y. Wu, N. Ye and G. Peng, *Angew. Chem., Int. Ed.*, 2023, **62**, e202217039.
55 A. B. Garg, D. Vie, P. Rodriguez Hernandez, A. Muñoz, A. Segura and D. Errandonea, *J. Phys. Chem. Lett.*, 2023, **14**, 1762–1768.
56 W. Jin, W. Zhang, A. Tudi, L. Wang, X. Zhou, Z. Yang and S. Pan, *Adv. Sci.*, 2021, **8**, 2003594.
57 D. Errandonea, H. Osman, R. Turnbull, D. Diaz Anichtchenko, A. Liang, J. Sanchez Martin, C. Popescu, D. Jiang, H. Song and Y. Wang, *Mater. Today Adv.*, 2024, **22**, 100495.
58 H. L. Wells, *Z. Anorg. Chem.*, 1892, **2**, 402–419.
59 V. I. Pakhomov, P. M. Fedorov, Y. A. Polyakov and V. V. Kirilenko, *Zh. Neorg. Khim.*, 1977, **22**(1), 188–192.
60 R. Sjovall and C. Svensson, *Acta Crystallogr., Sect. C: Struct. Chem.*, 1988, **44**, 207–210.
61 M. Kars, T. Roisnel, V. Dorcet, A. Rebbah and O. L. Carlos, *Acta Crystallogr., Sect. E: Struct. Rep. Online*, 2012, **68**, i11–i11.
62 O. Parasyuk, O. Khyzhun, M. Piasecki, I. Kityk, G. Lakshminarayana, I. Luzhnyi, P. Fochuk, A. Fedorchuk, S. Levkovets and O. Yurchenko, *Mater. Chem.*, 2017, **187**, 156–163.
63 A. A. Lavrentyev, B. V. Gabrelian, V. T. Vu, P. N. Shkumat, G. L. Myronchuk, M. Khvyshchun, A. O. Fedorchuk, O. V. Parasyuk and O. Y. Khyzhun, *Opt. Mater.*, 2015, **42**, 351–360.
64 Y. Chu, P. Wang, H. Zeng, S. Cheng, X. Su, Z. Yang, J. Li and S. Pan, *Chem. Mater.*, 2021, **33**, 6514–6521.
65 Y. Li, M. Wang, T. Zhu, X. Meng, C. Zhong, X. Chen and J. Qin, *Dalton Trans.*, 2012, **41**, 763–766.
66 G. Han, Y. Wang, X. Su, Z. Yang and S. Pan, *Sci. Rep.*, 2017, **7**, 1901.
67 J. Li and F. L. Deepak, *Chem. Rev.*, 2022, **122**, 16911–16982.
68 B. Zhang, G. Shi, Z. Yang, F. Zhang and S. Pan, *Angew. Chem., Int. Ed.*, 2017, **56**, 3916–3919.
69 L. Wang, D. Chu, Z. Yang, J. Li and S. Pan, *Chem. Sci.*, 2024, **15**, 6577–6582.
70 X. Wang, J. Li, Z. Zhao, S. Huang and W. Xie, *J. Appl. Phys.*, 2012, **112**, 023701.
71 L. Luo, L. Wang, J. Chen, J. Zhou, Z. Yang, S. Pan and J. Li, *J. Am. Chem. Soc.*, 2022, **144**, 21916–21925.
72 T. Ouahrani, R. M. Boufatah, M. Benaissa, Á. Morales-García, M. Badawi and D. Errandonea, *Phys. Rev. Mater.*, 2023, **7**, 025403.
73 F. Li, S. Pan and Z. Yang, *Mater. Chem. Front.*, 2021, **5**, 7580–7586.

74 X. Gonze, B. Amadon, P. M. Anglade, J. M. Beuken, F. Bottin, P. Boulanger, F. Bruneval, D. Caliste, R. Caracas, M. Côté, T. Deutsch, L. Genovese, P. Ghosez, M. Giantomassi, S. Goedecker, D. R. Hamann, P. Hermet, F. Jollet, G. Jomard, S. Leroux, M. Mancini, S. Mazevet, M. J. T. Oliveira, G. Onida, Y. Pouillon, T. Rangel, G. M. Rignanese, D. Sangalli, R. Shaltaf, M. Torrent, M. J. Verstraete, G. Zerah and J. W. Zwanziger, *Comput. Phys. Commun.*, 2009, **180**, 2582–2615.